

Research article

Elucidating the synergistic interactions of macroalgae and cellulose nanofibers on the 3D structure of composite bioaerogel properties

Rayan Y. Mushtaq¹, Azfaralariff Ahmad², Abdul Khalil H.P.S.^{2,3*}, Rana Baker Bakhaidar⁴,
Waleed Y. Rizg⁴, Shazlina Abd Hamid⁵, Abdulmohsin J. Alamoudi⁶, Che Ku Abdullah^{2,3},
Tata Alfatah⁷

¹Department of Pharmaceutics, College of Clinical Pharmacy, Imam Abdulrahman Bin Faisal University, 31441 Dammam, Saudi Arabia

²Green Biopolymer, Coatings and Packaging Cluster, School of Industrial Technology, Universiti Sains Malaysia, 11800 Gelugor, Penang, Malaysia

³Bioresource Technology Division, School of Industrial Technology, Universiti Sains Malaysia, 11800 Gelugor, Penang, Malaysia

⁴Department of Pharmaceutics, Faculty of Pharmacy, King Abdulaziz University, 21589 Jeddah, Saudi Arabia

⁵Nasdeem Ventures Sdn. Bhd., Taman Perindustrian Bukit Minyak, 14100 Simpang Ampat SPT, Penang, Malaysia

⁶Department of Pharmacology and Toxicology, Faculty of Pharmacy, King Abdulaziz University, 21589 Jeddah, Saudi Arabia

⁷Environment and Forestry Office of the Provincial Government of Aceh, 23239 Banda Aceh, Indonesia

Received 4 March 2024; accepted in revised form 29 April 2024

Abstract. Seaweed from macroalgae and cellulose from nonwood materials have gained attention in various fields. This study explores how seaweed and cellulose nanofibers (CNF) interact to form 3D networks in composite bioaerogels. The ratio of CNF and seaweed was varied to see how it affects the aerogel's inside and its properties. The observations show that the biocomposite aerogel is more rigid and shrinks less than using a single biopolymer. The CNF aerogel has a fine, thin network structure, and the seaweed aerogel has a thin sheet structure. The biocomposite aerogel combines both a fine network and a thin sheet structure. The composite aerogel's mechanical properties are significantly influenced by seaweed composition. The introduction of CNF increases elasticity, while seaweed enhances firmness. Generated computer modelling revealed that the abundant hydroxyl groups in CNF facilitated the formation of intermolecular bonds with seaweed. The bonding led to increased adhesion and entanglement between biopolymers, consequently enhancing elasticity and establishing a stable intermolecular interaction. The 3D X-ray imaging model shows that the skeletal framework primarily consists of seaweed biopolymer, with CNF serving to reinforce this structure thus enhancing the mechanical properties and robustness of the composite bioaerogels.

Keywords: bioaerogel, seaweed, cellulose nanofibers, 3D X-ray imaging, supercritical CO₂

1. Introduction

Aerogels, known for their outstanding attributes, offer substantial potential in a wide range of medical and non-medical applications [1]. They exhibit exceptional characteristics such as high porosity, an

extensive specific surface area, extraordinarily low density, and a unique open-pore structure featuring interconnected meso- and macropores [2, 3]. These characteristics make them suitable for various applications such as air filters, water purification, drug

*Corresponding author, e-mail: akhalihps@gmail.com

© BME-PT

carriers, wound dressings, thermal insulation, and many more [4–7]. Although aerogels can be produced from either organic or inorganic materials, in recent years, aerogel materials based on biopolymers such as cellulose, chitosan, starch, seaweed, *etc.*, have attracted the attention of researchers worldwide due to their environmental compatibility [6]. Among biopolymers, cellulose has been considered an attractive material for producing bioaerogels due to its advantages, including low cost, lightweight nature, and high processability [8].

As a derivative of cellulose, cellulose nanofibers (CNF) have gained significant attention due to their renewable nature, biodegradability, and excellent mechanical properties at the nanoscale [9, 10]. Due to remarkable attributes such as low thermal expansion, an extraordinary aspect ratio, enhancing effects, and exceptional mechanical and optical properties, CNF has been explored in various fields, including materials science, biotechnology, and medicine, for innovative and sustainable applications [11–13]. This makes them versatile candidates for applications ranging from nanocomposites to security papers and food packaging [14]. Incorporating CNF into polymers to fabricate nanocomposite aerogels has proven to be a pivotal strategy, leading to nanocomposites with significantly enhanced mechanical performance.

Alongside cellulose, seaweed is a renewable resource rich in polysaccharide biopolymers such as alginate, carrageenan, fucoidans and agar [15]. Seaweed-based biopolymer has garnered considerable attention in recent years and is widely utilized for numerous advanced applications, serving as one of the most sought-after sources of cost-effective polysaccharide materials [16, 17]. It has the ability to form biopolymers with high surface areas and super absorbent behavior and is impervious to fats and oils [18, 19]. These biopolymers are derived from different types of seaweed and have unique properties that make them valuable in various applications, ranging from food products to biomedical materials. Among seaweed polysaccharides, carrageenan, a red seaweed-based polysaccharide, has gained much attention in developing bio-based food packaging film due to its excellent film-forming ability [20]. Kappa carrageenan, derived from *Kappaphycus alvarezii* or *Eucheuma denticulatum*, is the most popular and widely used among the three types of carrageenan—kappa, iota, and lambda—owing to its superior gel-forming capabilities [15, 20]. However, like other

biopolymers, this biopolymer has relatively lower mechanical strength compared to conventional non-renewable polymers [21]. Thus, they are frequently blended with other materials to improve their properties.

While existing research has extensively explored the combination of cellulose nanofibers (CNF) with various biopolymers (such as chitosan, seaweed, sodium alginates, and gelatin) [22–25] primarily to enhance specific properties for targeted applications, these studies often do not address the intricacies of the 3D network structures or the complex interactions between nanocellulose and the biopolymers. This study uniquely focuses on these interactions between CNF produced via supercritical CO₂-assisted techniques and a specific biopolymer, kappa-carrageenan, using advanced 3D X-ray imaging to examine how varying ratios affect the aerogel's internal structure and its mechanical properties. This approach allows us to explore the impact of varying CNF and seaweed concentrations on the composite's architecture. This pioneering use of 3D X-ray imaging marks the first instance of employing this technology to elucidate the interaction dynamics between these two biopolymers, enhancing our understanding of their complex 3D architecture and potentially optimizing the material's properties for diverse applications. This innovative characterization technique provides researchers with the means to visualize and quantify the detailed 3D architecture of the aerogels, offering new insights into the fundamental properties that govern their functionality in various fields.

2. Materials and methods

2.1. Materials

Dried raw red seaweed (*Kappaphycus alvarezii*) was obtained from Green Leaf Synergy Sdn. Bhd. in Tawau, Sabah, Malaysia. Commercial cellulose nanofiber (CNF) was sourced from Cellulose Lab, Canada. The extracted CNF was derived from kenaf bast fiber collected from Nibong Tebal Paper Mills in Seberang Perai, Pulau Pinang, Malaysia.

2.2. Preparation of seaweed biopolymer

The dried seaweed was cleaned to remove dirt, impurities, and sand particles from its surface. Subsequently, the seaweed was soaked in distilled water at a ratio of 1 to 10 (w/v) for 2–5 h at room temperature. After soaking, the material was chopped into small pieces using a food blender and then dried in

an oven for 2–3 days at 40 °C. The dried seaweed was ground to a size of 500 μm using an MF10 Microfine grinder drive (IKA, Germany) and then stored in vacuum-sealed plastic bags for later use.

2.3. Isolation of cellulose nanofiber

Kenaf bast fiber had a purification process prior to nanocellulose extraction, which involved three main steps: pulping, bleaching, and defibrillation. Initially, raw kenaf bast was dried in an oven at 100 °C for 24 h. Then, 300 g were cut into 2–3 cm lengths and immersed in a 2.1 l of NaOH (26% w/w of bast) followed by cooking at 170 °C for 90 min. The pulp was then washed and air-dried for subsequent stages. The kenaf pulp underwent a double purification process, starting with a 3 stage bleaching procedure as described by Nasution *et al.* [26]. The bleached pulp then underwent supercritical carbon dioxide (SC-CO₂) treatment (60 °C with 50 MPa) for 2 h. Finally, the fibers underwent a mild hydrolysis process using a 13% oxalic acid solution at a 1:20 ratio (w/v), followed by homogenization at 10000 rpm using an Ultra-turrax homogenizer (IKA, Germany) for 3 h. The resulting suspension was then stored at 4 °C for future use. Figure 1 illustrates the process for obtaining CNF with supercritical CO₂ treatment.

The CNF obtained was analyzed for particle size distribution and zeta potential and observed by transmission electron microscopy (TEM). The particle size distribution and zeta potential of the CNF suspension

were measured using a Zetasizer Nano (Malvern Instrument, United Kingdom). To ensure thorough dispersion, the CNF suspensions were sonicated for 15 min prior to testing. Morphological analysis was conducted using a Philips CM12 TEM instrument. For sample preparation, the CNF suspension was first sonicated and then treated with uranyl acetate for 15 min, followed by immersion in drops of distilled water for 30–60 s. The samples were then placed on slot grids, positioned in the chamber, and prepared for observation. Staining with uranyl acetate was utilized to enhance the contrast of the ultrathin CNF samples.

2.4. Preparation of CNF-Seaweed composite aerogel

Two stock aerogel-forming solutions were prepared, one containing 3% CNF and the other 3% seaweed. The CNF was dispersed in water at room temperature and homogenized at 10000 rpm using an Ultra-turrax homogenizer (IKA, Germany) for 3 h. Simultaneously, the seaweed powder was dissolved by heating for 2 h at 90 °C with continuous stirring until all the seaweed dissolved.

From these stock solutions, they were mixed as specified in Table 1. The combined solution was then thoroughly stirred with a magnetic stirrer and poured into a 50 ml cylindrical mould. Following mixing, the aerogel-forming solution was frozen at –40 °C for 24 h and subsequently subjected to a freeze-drying process for 72 h.

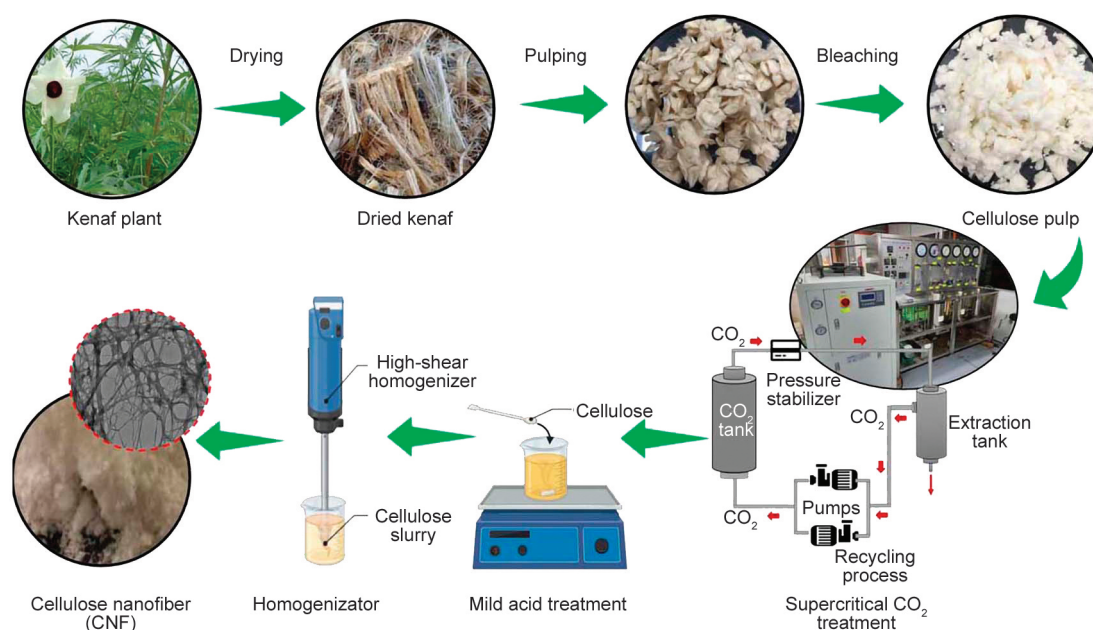


Figure 1. The process for obtaining CNF with supercritical CO₂ treatment.

Table 1. Aerogel and composite aerogel mixing formulation.

3% CNF solution [ml]	3% seaweed solution [ml]	Volume water [ml]	Theoretical total solid content [g/50 ml]	Sample code
40	–	10	1.2	CNF
–	40	10	1.2	Seaweed
20	20	40	1.2	1C:1S
20	60	–	2.4	1C:3S
30	30	–	2.4	3C:3S
60	20	–	2.4	3C:1S

2.5. Physical characterization

The obtained aerogels were observed and characterized in terms of weight, volume, shrinkage, density, porosity and water absorption capacity. The shrinkage was calculated by dividing its theoretical volume (50 cm³) by its actual volume, while the density of each aerogel was calculated by dividing its mass by its volume.

Porosity is a measure of the empty space within a material and is an important characteristic of aerogels. The porosity was calculated using the Equation (1):

$$\text{Porosity [\%]} = \left(1 - \frac{\text{Calculated density}}{\text{Theoretical density}}\right) \cdot 100 \quad (1)$$

where the density of CNF was 1.4 g/cm³ while carrageenan was 1.9 g/cm³ [27, 28]. The density for CNF and carrageenan blend was estimated to be 1.65 g/cm³. The water absorption capacity of the aerogels was evaluated, as reported by Mawardi *et al.* [29]. The pre-determined weight of each aerogel was immersed in 20 ml of distilled water for 1 h. Afterward, the aerogels were taken out of the water, and excess water was removed by pressing them gently against filter paper. The fully saturated aerogels were subsequently weighed. The water absorption capacity was calculated based on weight changes according to Equation (2):

$$\begin{aligned} \text{Water absorption capacity} \left[\frac{\text{g}}{\text{g}} \right] &= \\ &= \frac{\text{wet weight} - \text{dry weight}}{\text{dry weight}} \end{aligned} \quad (2)$$

2.6. Fourier-transform infrared analysis (FT-IR)

FT-IR analysis was conducted for all the aerogel samples to examine the surface functional groups. The analysis was performed using a Thermo Scientific model Nicolet I S10 spectrometer (Thermo Fisher

Scientific, Waltham, MA, USA), which allowed the investigation of specific organic functional groups on the surface. Spectra were recorded in the range of 4000 to 400 cm⁻¹ at room temperature, with a resolution set at 4 cm⁻¹.

2.7. Field emission scanning electron microscopy (SEM)

The morphological analysis of all prepared aerogel samples was conducted using field emission scanning electron microscopy (FEI Quanta FEG 650, Thermo Fisher Scientific, Eindhoven, The Netherlands). Accelerating voltages ranging from 0.5 to 30 kV were applied. A platinum coater was utilized for superior electrical conductivity during the characterization process.

2.8. Mechanical analysis

The compression properties of the aerogel were assessed using a universal texture analyzer TA HD plus C (Stable Micro Systems Ltd., Surrey, England) equipped with a 5 kg load cell and 20 mm compression plate. The aerogel was compressed with a probe set at a speed of 0.5 mm/s and an applied force of 3.5 N for 60 s. This analysis provided data on the aerogel's compression properties, specifically hardness [N] and springiness [m], calculated by the software.

2.9. Thermogravimetric analysis (TGA)

Thermal composition and thermal stability analyses of all the aerogels were conducted using thermogravimetric analyzer TGA/SDTA 851e (Mettler-Toledo International Inc., Columbus, OH, USA). The temperature range tested was from 50 to 800 °C, with a heating rate of 10 °C/min under a nitrogen atmosphere.

2.10. Computer simulation

The molecular structures of two biopolymers, specifically κ -carrageenan (PubChem CID: 481108992)

and cellulose (PubChem CID: 16211032), were analyzed in both 2D and 3D formats. These structures were obtained from the PubChem Compound Database (National Center for Biotechnology Information; <https://pubchem.ncbi.nlm.nih.gov/>) on September 9, 2023.

The biopolymer files were prepared using BIOVIA Discovery Studio Visualizer version 20.1.0 (Dassault Systemes BIOVIA), while the interaction analysis was conducted through Autodock Vina docking using PyRx biological software v0.8 (<https://pyrx.sourceforge.io>, accessed on September 10, 2023). Autodock Vina is a free, open-source tool specifically designed to quickly assess the binding affinity between a ligand and targeted molecules [30]. The interactions were then visualized using the Discovery Studio Visualizer.

2.11. 3D Network analysis

The aerogels were scanned using the nanoVoxel-3000 series X-ray 3D microscope (Tianjin San Ying Precision Instrument Co., Ltd., Tianjin, China). This instrument utilizes a transmission target ray source and boasts sub-micron resolution, along with advanced 3D imaging capability. Its transmissive tube-open X-ray source system allows high-resolution testing, particularly for medium and low-density samples, ensuring the generation of excellent computed tomography (CT) scan images.

Following the CT scanning, the acquired images undergo additional processing, which involves contrast

adjustment, scatter dots noise filtration, and image segmentation using VG Studio Max (Volume Graphics, Hockenheimring, Germany).

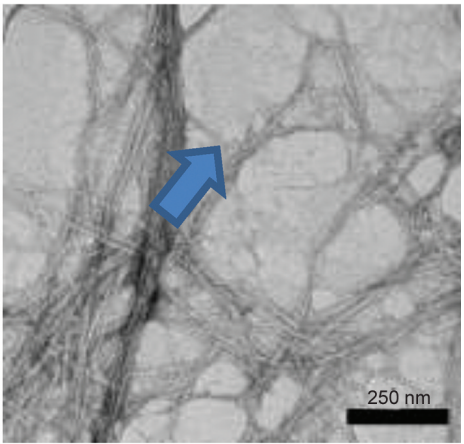
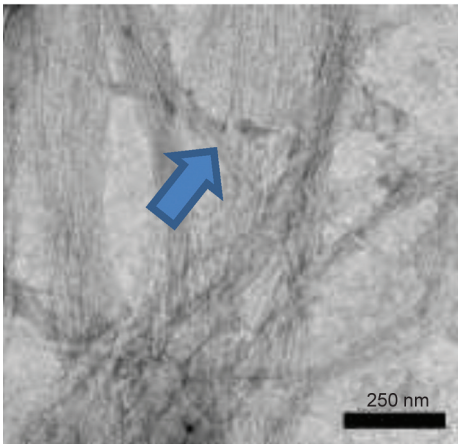
3. Results and discussion

3.1. Characterization of isolated CNF

The particle size and zeta potential of extracted CNF with and without SC-CO₂ treatment in comparison to the commercial CNF are presented in Table 2. The peak intensity reflects the intensity-weighted distribution of the CNFs, as determined by laser diffraction during the analysis [31]. Particle size analysis of the isolated nanocellulose changed after supercritical treatment. However, SC-CO₂ treated CNF had lower diameter and mean size (19.7±1.1 and 59.4±3.4 nm respectively) compared with the untreated CNF (48.0±2.3 and 98.6±4.8 nm). The particle size of CNF is slightly larger compared to that in the previous study, which reported sizes of 7.14 and 53.72 nm using the same method to obtain CNF from carpet waste fiber [27]. The use of high pressure during SC-CO₂ treatment assists the CO₂ in penetrating the fiber structure and removing the lignin and impurities, thus producing purer CNC and smaller particles [27]. The TEM images provided a detailed visualization of the nanofiber distribution, showcasing the diverse range of fiber diameters and the degree of dispersion within the samples.

Notably, the CNFs treated with SC-CO₂ exhibited a pronounced shift towards smaller particle sizes compared to untreated CNFs. This shift is attributed to

Table 2. Size distribution, zeta potential, and TEM images of CNF treated and untreated with SC-CO₂.

Sample		SC-CO ₂ Treated CNF	Untreated CNF
Diameter	[nm]	19.7±1.1	48.0±2.3
Mean size	[nm]	59.4±3.4	98.6±4.8
Peak intensity	[%]	17.6±1.6	14.8±0.9
Zeta potential	[mV]	-33.9±2.5	-33.1±1.9
TEM image			

the SC-CO₂ treatment's ability to disrupt the cellulose fibers, enhancing their breakdown into finer nanofibers. Importantly, all zeta potential measurements exceeded –30 mV, suggesting a notably stable suspension in water [32]. The SC-CO₂-treated CNFs demonstrated the highest zeta potential, indicating superior suspension stability. This enhanced stability is likely due to the SC-CO₂ treatment facilitating fiber defibrillation, which increases the surface area for interaction with chemicals during hydrolysis. Furthermore, SC-CO₂ treatment promotes more effective dispersion of nanofibrils in the homogenization process, contributing to the observed increase in suspension stability. These findings underscore the potential of SC-CO₂ treatment as a pivotal technique for improving the functional properties of CNFs, particularly in applications requiring stable aqueous suspensions.

3.2. Physical characterization of aerogels

The aerogels produced were cylindrical in shape, with varying sizes and thicknesses. It was observed that the aerogels experienced shrinkage compared to the original dimensions of the cylinder mold, which had a diameter and thickness of 4 cm each. The physical characteristics of the aerogels are recorded in Table 3.

CNF and seaweed aerogels display distinct characteristics, such as differences in density and water absorption capacities. Notably, all aerogels shrink in size after drying, resulting in a reduction in volume from the initial aerogel-forming solution of approximately 50 cm³. The volumes of the dried aerogels vary between 25 and 40 cm³, indicating a volume shrinkage ranging from 21 to 48%. Specifically, the seaweed aerogel exhibits more significant shrinkage, at 44.94%, compared to the CNF aerogel, which shrinks by 32.27%. As a result, the seaweed aerogel demonstrates a higher density than the CNF aerogel.

The solid content and the type of biopolymer used play crucial roles in the formation of aerogels, directly influencing their structural characteristics and behavior during shrinkage. As the aerogel shrinks, it generally indicates a loss of porosity and an increase in density, which can affect the mechanical strength and other properties of the aerogel. Specifically, shrinkage can lead to a denser structure, potentially increasing the mechanical strength but reducing other properties due to decreased pore volume [33]. To correlate shrinkage with material properties, it is essential to measure changes in porosity and density. A comparative analysis of three different building materials – seaweed, CNF, and a composite of both – revealed distinct differences in behavior based on solid content. Specifically, the seaweed aerogel exhibited the most significant shrinkage, registering at 44.94±0.76%, which was notably higher than that observed in the CNF aerogel, which shrank by 32.27±1.57%. The composite aerogel, composed of CNF and seaweed at a 1:1 ratio, demonstrated moderate shrinkage. The biopolymer interactions and their respective solid contents significantly influence the structural integrity and dimensional stability of aerogels [34]. Unlike CNF, which is insoluble in water, seaweed biopolymer is water-soluble. This solubility plays a crucial role during the drying process of the aerogel, as the loss of water causes the biopolymer chains to merge [35]. As the aerogel transitions from a gel to a solid state, the biopolymer's stiffness increases and the connections between chains tighten due to bond hardening. In contrast, the inherent physical structure of CNF prevents collapse, maintaining the integrity of the aerogel structure throughout the drying process.

Composite aerogels (1C-1S, 1C-3S, 3C-3S, 3C-1S) exhibit variations in properties based on different ratios of CNF to Seaweed. With less solid content, the 1C-1S aerogel experiences greater shrinkage but has

Table 3. Physical properties of the obtained aerogel and composite aerogel.

Aerogel	Dry weight [g]	Theoretical volume [cm ³]	Volume [cm ³]	Shrinkage [%]	Density [g/cm ³]	Porosity [%]	Wet weight [g]	Water adsorption capacity [g/g]
CNF	1.23±0.06	50	34.05±0.79	32.27±1.57	0.036±0.001	97.41±0.09	25.3±0.7	19.4±3.2
Seaweed	1.22±0.06	50	27.68±0.38	44.94±0.76	0.044±0.001	97.67±0.06	10.4±0.9	7.2±2.7
1C-1S	1.24±0.02	50	31.26±0.75	37.81±1.50	0.040±0.001	97.59±0.13	17.2±0.5	12.7±3.5
1C-3S	2.44±0.03	50	33.74±0.43	32.87±0.86	0.072±0.001	95.62±0.03	28.6±0.7	10.5±2.9
3C-3S	2.42±0.02	50	37.27±0.50	25.85±1.02	0.065±0.001	96.05±0.03	32.5±0.8	12.2±2.1
3C-1S	2.43±0.02	50	39.31±0.57	21.79±1.14	0.062±0.001	96.25±0.08	35.3±0.6	13.4±3.6

a lower density compared to the other composite aerogels. Among the three composite aerogels with the same solid content, the highest density and lowest porosity were recorded for the 1C-3S aerogel due to its high shrinkage. It was found that increasing CNF content leads to reduced shrinkage and, consequently, reduced density. The decrease in volume and increase in density suggest a denser arrangement of the biopolymer network tightly packed within the aerogel structure [29, 36]. The Seaweed aerogel exhibited a higher density compared to the CNF aerogel, even though they had the same solid content. This difference can be attributed to greater shrinkage (44.49%) in the Seaweed aerogel. The 3C-1S aerogel demonstrated the highest volume, lowest shrinkage, lowest density, and highest porosity among composite aerogel with the same weight. The inclusion of more CNF creates a supportive network within the aerogel, which helps maintain its structure by reducing shrinkage and thereby increasing porosity. Similar findings have been reported in other studies, where highly flexible nanofibrillated cellulose chains were found to entangle and form a random network-like structure due to hydrogen bonding both within and between molecules [33].

The CNF aerogel exhibits a water adsorption capacity of 25.3 ± 0.7 g of water, indicating its ability to absorb and retain water, constituting 19.4 ± 3.2 g/g of its dry weight. Similar value (19.1 ± 6.2 g/g) has been reported for the aerogel made using CNF aerogel [37]. The water is trapped in the formed pores of the CNF aerogel. In comparison to the seaweed aerogel, a lower water absorption capacity was recorded 7.2 ± 0.3 g/g. This is attributed to the swelling of the seaweed network and its stickiness, causing structural shrinking and agglomeration. Consequently, introducing more seaweed biopolymer into the formulation reduces the water absorption capability of the composite aerogel.

3.3. Characterization of composite aerogel using FT-IR

IR spectroscopy is a robust, non-destructive analytical method to evaluate the structure of the composite aerogel component and the interaction between them. The FTIR spectra of CNF, seaweed, and CNF-Seaweed aerogel composites are presented in Figure 2. As κ -carrageenan is a linear polysaccharide with alternating 3-linked- β -D-galactopyranose and 4-linked- α -D-galactopyranose units, and cellulose has a

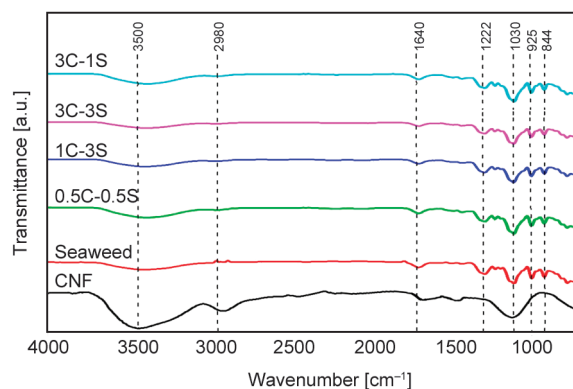


Figure 2. FT-IR spectrum of biopolymer and biocomposite aerogel.

structure with β -(1 \rightarrow 4)-D-glucopyranose repeat units, both polysaccharides consist of glucopyranose repeating units [38]. Consequently, the IR spectra of these polysaccharides exhibit some similarities.

Both biopolymers exhibit a broad band in the spectral region between 3700 and 3000 cm^{-1} , corresponding to the O–H stretching vibrations. Additionally, a small peak in the range of 3000 to 2800 cm^{-1} is assigned to the symmetric and asymmetric stretching vibrations of C–H and C–H₂ groups. All samples show spectral bands at 1639 cm^{-1} assigned to the deformation vibration of OH groups absorbed water [38]. The band from 1033 cm^{-1} is assigned to C–O–C stretching vibration, while the other two bands are associated with the OH groups present in the structure of both κ and CNC. For the FTIR spectrum of seaweed and composite aerogel, a moderately strong band around 845 cm^{-1} was attributed to C–O–SO₄ on C4 of galactose-4-sulfate (G4S). The two bands at approximately 925 and 1030 cm^{-1} indicated the presence of 3,6-anhydrogalactose (DA), while the presence of a band around 122 cm^{-1} suggested the presence of a sulfate ester [39]. Due to the similarities between the components in the blends, the IR spectra of the composite aerogels are very similar to the seaweed spectrum [38].

3.4. Morphology and microstructural of composite aerogel

Figure 3 displays images of the formed aerogels prepared with varying ratio, showcasing their real surface and microstructure observed under SEM. CNF aerogels are visually white, while seaweed-based aerogels exhibit a distinctive brownish hue. In comparison, composite aerogels display a cream coloration, influenced by the natural brown hue of the

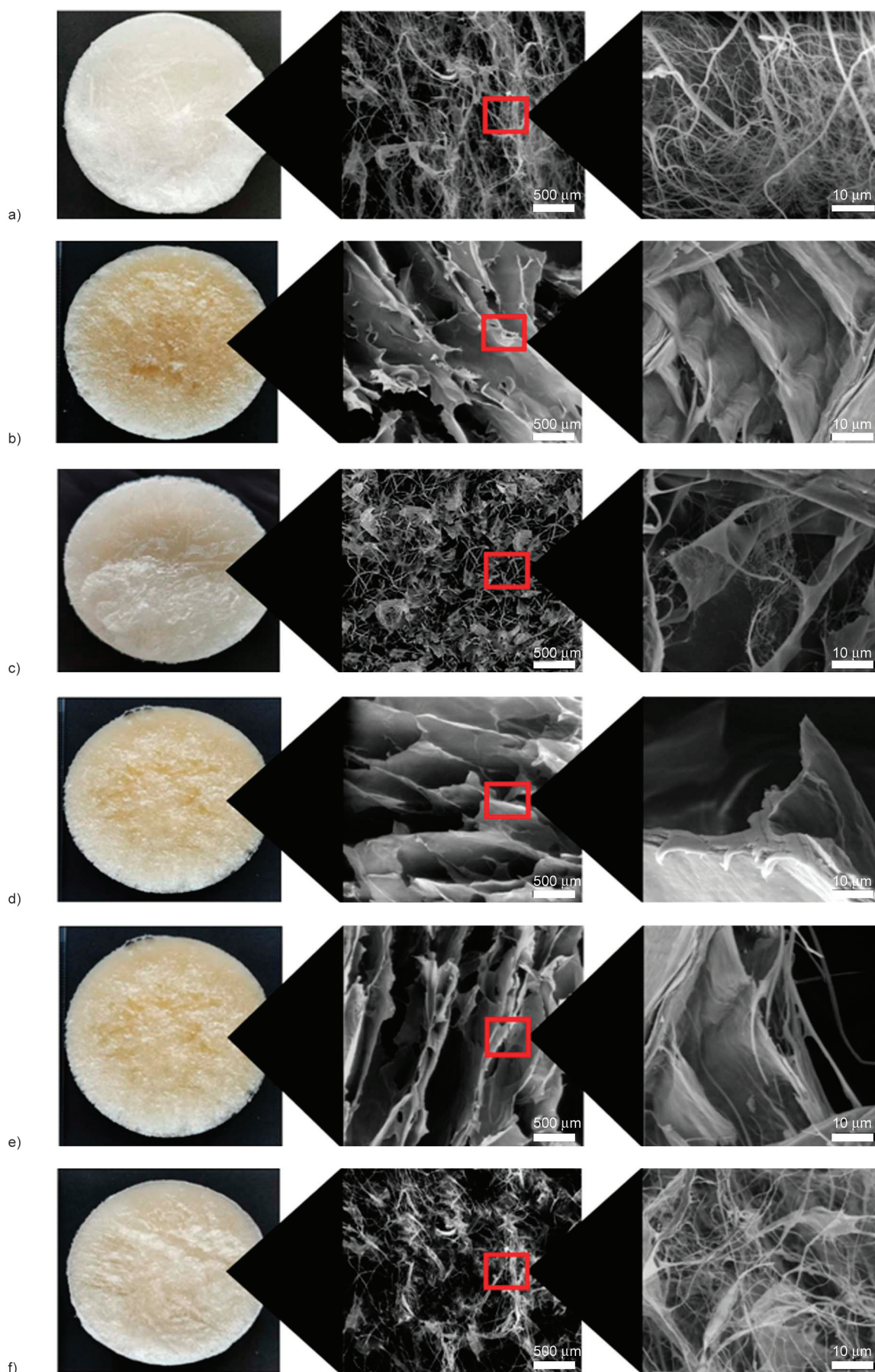


Figure 3. Image of prepared aerogel and composite CNF-Seaweed aerogel (real image, 100× magnification and 5000× magnification): a) CNF; b) seaweed; c) 1C-1S; d) 1C-3S; e) 3C-3S; and f) 3C-1S.

seaweed. The porosity of these aerogels can be clearly seen from the SEM images, which present large macro- and mesopores (ranging from several hundred nanometers to several micrometers). This is typical for bioaerogels and results from the formation of bulky ice crystals during freezing [40]. Direct freeze-drying commonly leads to foam-like structures characterized by a higher presence of macropores compared to micropores [41]. Further detailed analysis was conducted on the SEM image.

At both low magnification (100×) and high magnification (5000×), both biopolymers form aerogels differently: CNF aerogels create a thin network structure resembling an interconnected lattice of fibers (Figure 3a). In contrast, the seaweed aerogel is composed of stacked and interconnected layers (lamellae) of seaweed material, forming a unique structure of delicate thin sheets that resemble cellular structures or clusters, as shown in Figure 3b. This intricate arrangement of lamellae creates a complex, layered, and interconnected framework that enhances the architectural complexity of the seaweed aerogel. This structural distinctiveness contributes to the lower mechanical properties of CNF aerogel, which lacks the entangled, robust framework present in seaweed aerogel, rendering it more vulnerable to relative displacement [41]. The introduction of either CNF or seaweed, whether at a low (1) or high (3) ratio, results in a significant transformation in the microstructures of the aerogels. In the case of aerogel 1C-1S (Figure 3c), both fibers and lamellae constitute the overall structure of the aerogel. On the other hand, aerogel 3C-1S, which has a higher

concentration of CNF (Figure 3f), exhibits a more prominent cellulose network compared to aerogel 1C-3S (Figure 3d). Despite both having a 1:1 ratio, aerogel 3C-3C (Figure 3e) displays a distinct denser microstructure when compared to aerogel 1C-1S (Figure 3c). It bears a closer resemblance to the seaweed aerogel, although it still contains some fibers. This variation can be attributed to differences in aerogel density.

3.5. Mechanical analysis

The mechanical properties of the composite aerogels, including hardness and springiness were displayed in Figure 4 respectively, which are crucial for the practical applications of the prepared aerogels. These properties are of significant importance as they are commonly used to compare the mechanical characteristics of various materials [42].

The hardness measurement of the seaweed aerogel showed a significant value of 2805 g, which is considerably higher than that of the CNF aerogel, which measured at 1271 g. This difference in hardness can be attributed to the shrinkage that occurs during the drying process, which results in the seaweed aerogel having a denser structure. Upon introducing varying ratios of CNF to the seaweed aerogel, the hardness decreased from the initial 2805 g (seaweed) to 1930 g (3C-3S). This reduction in hardness implies that the addition of CNF resulted in a decrease in the seaweed aerogel's overall hardness. Conversely, when more seaweed was incorporated into the CNF aerogel, the trend reversed. The hardness of the CNF aerogel increased from the initial value of 1271 g (CNF)

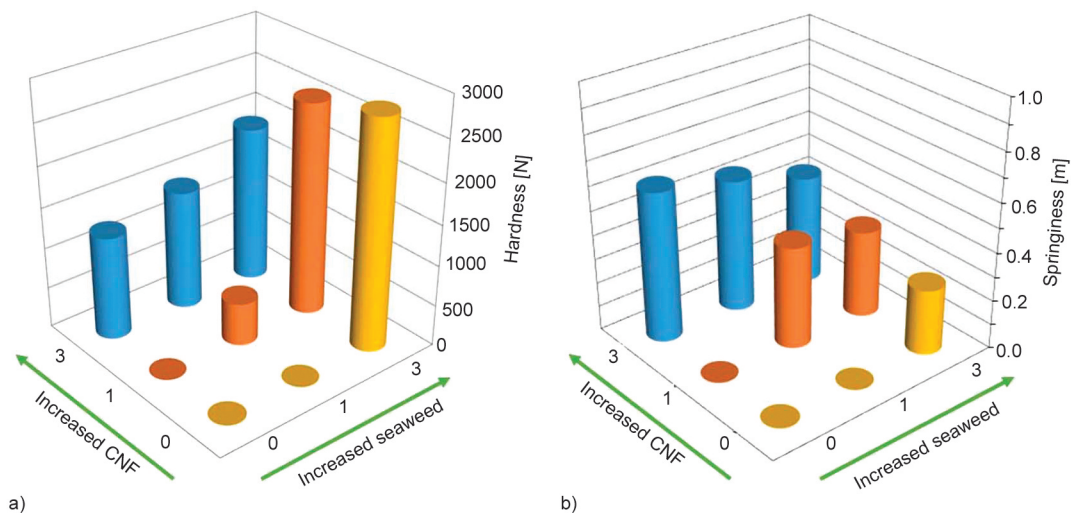


Figure 4. Characterization of CNF, seaweed and CNF-seaweed aerogels at different compositions: a) hardness and b) springiness.

to 1930 g (3C-3S), indicating that the inclusion of more seaweed enhanced the aerogel's hardness. It can be observed that a higher CNF ratio reduces the shrinkage of the composite aerogel, thus resulting in lower density, which affects the hardness. This is evidenced by the fact that even though samples 1C-1S and 3C-3S share the same ratio, the difference in density significantly influences their hardness.

The presence of CNF in the aerogel positively influenced its springiness and elasticity. The addition of CNF enhanced the aerogel's ability to regain its original shape after compression, increasing its elasticity and enabling it to withstand deformation without breaking. A springiness value approaching 1 signifies that the aerogel efficiently restored its original shape after compression, maintaining structural integrity even under pressure or deformation [43]. The introduction of CNF into the seaweed aerogel increased springiness from 0.16 (seaweed) to 0.38 (3C-3S). It has been reported that the tensile strength of CNF-seaweed film increases with rising CNF content up to the optimum concentration [44]. In contrast, inverse trends were observed when CNF aerogel was introduced with seaweed biopolymer, resulting in a decrease in the springiness of the CNF aerogel. All these changes in physical properties were influenced by the variation in the intensity of the aerogel.

3.6. Thermal analysis

Understanding the changes in thermal stability of composite aerogels is essential to broaden their possible applications. Various applications might demand distinct temperature tolerances, some requiring high thermal stability while others may not require such stringent conditions. Figure 5 presents

the analysis of thermal properties for CNF-Seaweed composite aerogels with different ratios conducted through TGA and derivative thermogravimetry (DTG). This assessment illustrates their response to heating from 60 to 800 °C at a rate of 10 °C/min. It was found that mixing CNF and seaweed biopolymer resulted in a change in the thermal properties of the composite aerogel. In general, across all samples, three distinct degradation temperatures were observed within three stages: below 150, 150–500 °C, and higher than 500 °C.

The weight loss observed in Stage I below 150 °C (Figure 5a) is attributed to the evaporation of water in the composite aerogel [29]. In Stage II, the devolatilization stage, the primary pyrolytic process took place, slowly releasing various volatile components and causing substantial weight loss. The initial temperature for thermal degradation in all composite aerogels was observed to range from 190 to 210 °C. Additionally, the temperatures for thermal degradation in all samples were noted to be between 200 and 220 °C. While seaweed generally decomposes at around 250 °C, previous research has shown that blending seaweed biopolymer with other polymers reduces its decomposition temperature [45]. This decomposition leads to the fragmentation of seaweed polymer chains, releasing sulfur dioxide and carbon dioxide [46]. Interestingly, as the proportion of CNF in the composite aerogel increases, a higher degradation temperature is observed, as shown in Figure 5b. The degradation process persists until about 500 °C. A minor peak, indicative of cellulose degradation, appears at around 350 °C, aligning with the optimal decomposition temperature for CNF [29]. This thermal degradation process involves the breakdown of glycosidic bonds in cellulosic components and additional

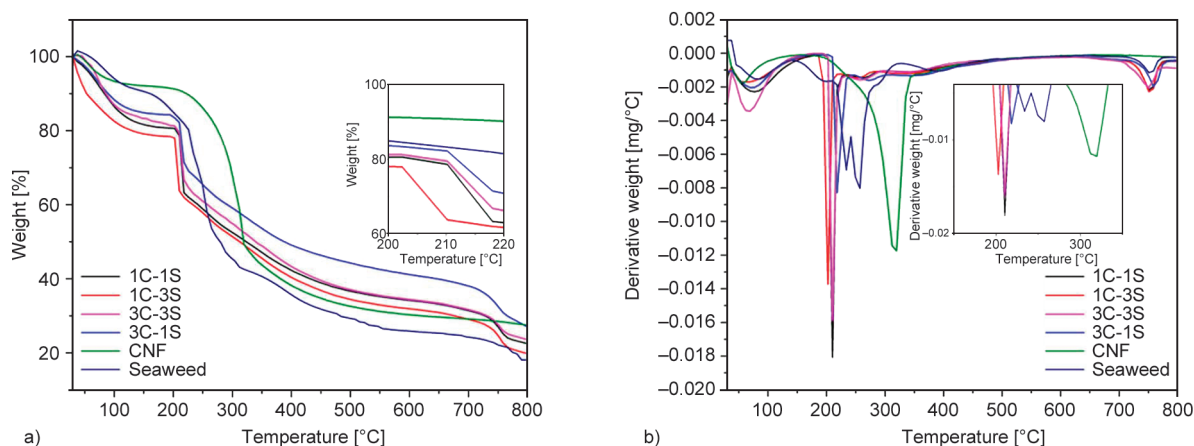


Figure 5. Thermal properties of composite aerogel: a) TGA thermogram, and b) DTG thermogram.

processes like decarboxylation, decarbonylation, and dehydration of seaweed constituents [47, 48]. However, the results indicate that although the composite aerogel demonstrates a higher degradation temperature with an increase in CNF, the small cellulose degradation peak suggests that the CNF might not be evenly distributed in the cellulose, with the predominant sample used in the thermal properties consisting of seaweed biopolymer.

In the third stage, above 500 °C, the residue slowly decomposed, resulting in the formation of a loose porous residue. During this process, secondary degradation was observed, as depicted by small peaks appearing at 750 °C (Figure 5) before reaching the completion of the decomposition process. It has been reported that carrageenan contains various inorganic salts. The carbonaceous residue within carrageenan may decompose at temperatures surpassing 600 °C [49]. The presence of these inorganic salts might contribute to the maximum weight loss peak observed in this range, potentially resulting from the pyrolysis of these salts.

The final thermal degradation residue shows that the composite aerogel having more cellulose has a higher residue. Sample with more seaweed (1C-3S) have lower ash residue. The ash residue increases from 19.78 to 29.03% as the ratio of CNF:seaweed increases from 1:1 to 3:1. It is important to note that samples 1C-1S and 3C-3S have similar ash residue since both have similar composition of biopolymer. It has been reported that the thermal stability of κ -carrageenan and cellulose nanocrystal composite film increases while a higher percentage of cellulose is introduced in the formulation [44]. In the same scenario, increasing the amount of CNF in the composite aerogel enhances its thermal stability, resulting in a higher ash residue. For every gram of CNF, there is a greater quantity of carbon ($C_6H_{10}O_5$) compared to carrageenan ($C_{12}H_{16}O_{15}S_2$). Carbon is renowned for its contribution to ash residue as carbonaceous material during thermal degradation [50]. Therefore, the elevated carbon content in CNF likely leads to increased ash residue and improved thermal stability seen in the composite aerogel.

3.7. Computational interaction simulation

Figure 6 illustrate the 2D and 3D structural models, respectively, of seaweed and cellulose nanofibers (CNF) and their combination. These figures detail the potential interactions between these components,

highlighting the molecular structures and suggesting how these materials might interact at a molecular level. Notably, the seaweed monomer features only four hydroxyl groups, whereas a cellulose monomer possesses six. The interaction between seaweed and CNF primarily occurs through hydrogen bonding, facilitated by the –OH groups present in both seaweed and CNF structures [51], as confirmed by previous FTIR studies. Additionally, CNF acts as a nano-reinforcing agent, playing a crucial role in improving the mechanical properties of the composite by controlling the movement of macromolecular chains during deformation. This enhancement is facilitated through the formation of strong interactions and hydrogen bonds between CNF and the seaweed biopolymer [52]. A previous study reported a notable enhancement in the tensile strength of seaweed film with the incorporation of microcrystalline cellulose (MCC) up to 5%. This improvement was attributed to the strong hydrogen bonding between MCC and the seaweed matrix, leading to improved compatibility and dispersion of MCC fillers within the matrix [22].

Moreover, it has been reported that the addition of cellulose as a filler is anticipated to strengthen the tensile strength and viscosity properties of the carrageenan matrix. This is achieved through the establishment of strong hydrogen bonds between carrageenan and the filler, thereby enhancing the mechanical strength of the biocomposite film and hard capsule [53]. These studies support the mechanical results obtained in our study, the addition of nanocellulose significantly supported the mechanical strength and hardness of the samples.

Understanding the hydrogen bonding structure in cellulose and seaweed is crucial as it forms the basis for developing advanced materials with specific properties and functionalities. Nair *et al.* [54] highlighted the robust network created by hydrogen bonds in CNF, making them excellent candidates for barrier applications in packaging. Similarly, Li *et al.* [55] research on carboxymethyl cellulose sodium film emphasized the importance of hydrogen bonds in influencing the material's properties. While most discussions revolve around biofilm, it's essential to recognize that the interaction between seaweed and CNF in aerogel formation follows similar principles. In this context, the combination of seaweed and cellulose constituents contributes to the unique structural properties of aerogels, offering potential applications

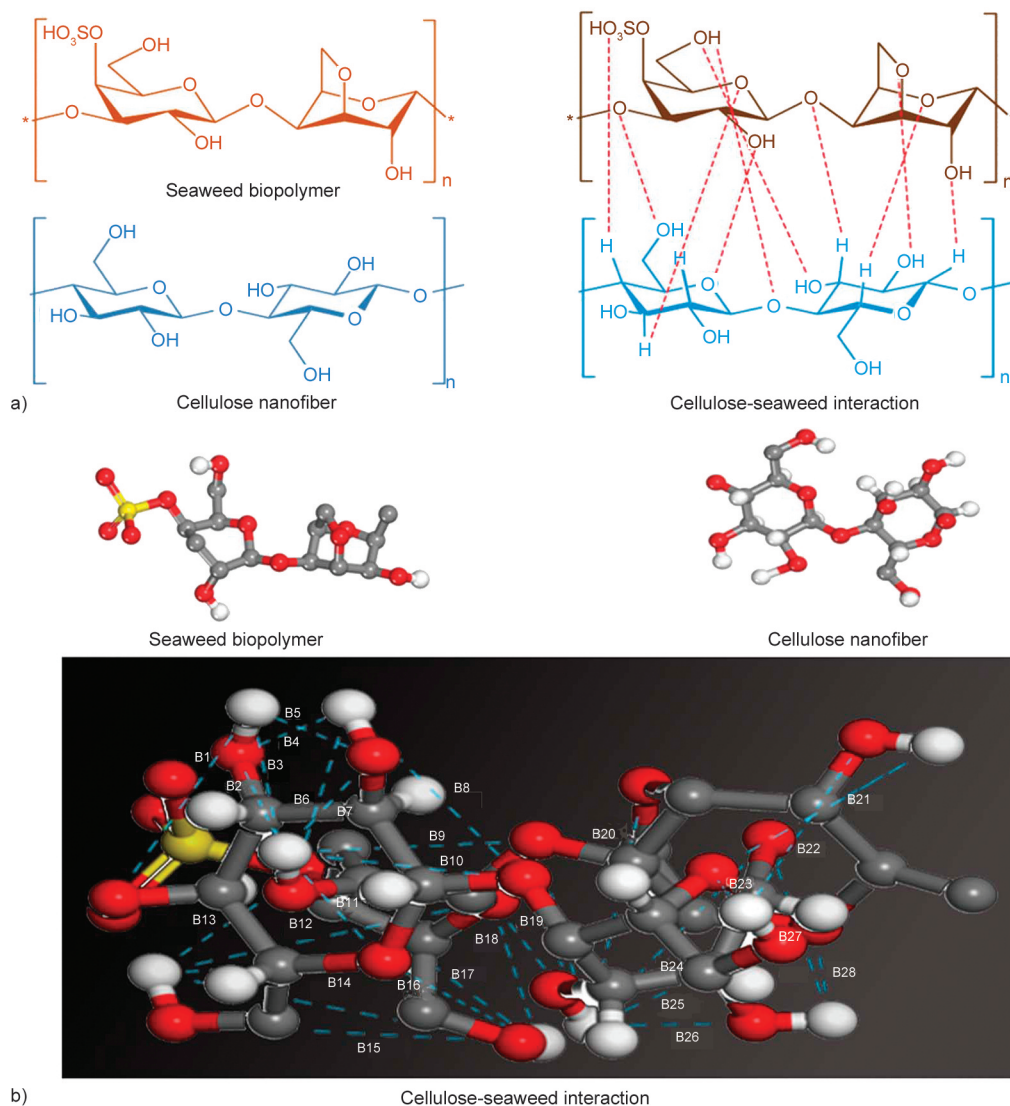


Figure 6. Representation of cellulose nanofiber, seaweed and their possible interaction illustrated in the form of a) 2D structure model and b) 3D structure model.

in various fields. The interaction between these materials, characterized by their distinct molecular structures and bonding capabilities, plays a fundamental role in shaping the final aerogel matrix.

Figure 6b illustrates the 3D interaction mechanism between seaweed and nanocellulose, with each bond labelled by a corresponding number. The blue dashed

line represents a hydrogen bond between atoms of different molecules. Hydrogen bonds are categorized into three types (Table 4). These bonds are typically classified as strong, moderate, or weak based on their bond length. Within the length range of 1.2–1.5 Å, hydrogen bonds demonstrate a moderate interaction strength, with a dissociation energy of 15–40 kcal/mol.

Table 4. General characteristics of the three major types of hydrogen bonds [57].

Interaction type	Strong	Moderate	Weak
Interaction force	Strongly covalent	Mostly electrostatic	Electrostatic/dispersive
Bond length [Å]	1.2–1.5	1.5–2.2	>2.2
Bond angles [°]	170–180	130–180	90–150
Bond energy [kJ/mol]	63–168	17–36	<17
Functional groups that form hydrogen bonds	[F–H–F] ⁻ [O–H–O] ⁻ [N–H–N]	N–H–O=C O–H P–O–H	C–H–O F–C C=C

Table 5. Computed hydrogen bond lengths estimated by Biovia, Materials Studio.

No. of bond	Length [Å]	No. of bond	Length [Å]
1	4.303	15	4.805
2	3.362	16	3.283
3	3.564	17	5.410
4	2.865	18	5.264
5	2.856	19	1.110
6	3.792	20	4.861
7	2.299	21	4.184
8	4.241	22	5.910
9	4.228	23	3.395
10	3.454	24	4.521
11	2.830	25	3.777
12	5.039	26	2.471
13	3.654	27	3.805
14	5.597	28	2.085

In the range of 1.5–2.2 Å, the interaction remains moderate but with a lower dissociation energy of 4–15 kcal/mol. Beyond 2.2 Å, the hydrogen interaction is considered weak, with a dissociation energy of less than 4 kcal/mol [56].

Through computer-generated models, it was determined that up to 28 potential hydrogen bonds could form. The lengths of these hydrogen bonds predominantly fall within the range of 2.085–5.910 Å. Table 5 provides a summarized overview of the length of various possible hydrogen bonds. The predominant bond length plays a crucial role in describing the bonding patterns within the weak and moderate hydrogen bond regimes based on the obtained results.

3.8. 3D structural interaction between seaweed and CNF

Figure 7 displays the real surface, simulated 3D molecular structure models and 3D X-ray image of CNF-seaweed composite aerogel prepared with various formulations. It can be observed that CNF prominently contributes to hydrogen bonds. More hydrogen bonds were established within the structure as the concentration of CNF increased in the mixtures, as shown in the 3D molecular structure model.

The 3D X-ray processed image clearly illustrates the composition of the aerogels, where green represents seaweed and red represents nanocellulose. As the concentration of seaweed increases, there is a corresponding increase in green areas, while an increase in CNF concentration leads to more red areas. This is consistent with findings from a study by Adam *et al.*

[58], which reported that the abundant hydroxyl groups in CNF form intermolecular bonds with carrageenan. These bonds contribute to enhanced viscosity, shear stress, and tensile strength of the material. Their finding supports our texture profile analysis (TPA) study; the hardness of our aerogel increases as the concentration of seaweed increases. This phenomenon might be evidenced by the heightened intensity and a shift in ¹H-NMR, indicating closer proximity of hydrogen atoms to electronegative atoms in both micro and nano-sized cellulose structures [59]. The interaction intensifies as the concentration of both seaweed and CNF increases, resulting in the formation of aerogel with high stability.

The molecular interaction between CNF and seaweed, as shown in Figure 7d, involves a complex network of hydrogen bonding and van der Waals forces [58]. Since nanocellulose, being rich in hydroxyl groups, forms hydrogen bonds with the polysaccharides present in seaweed, which occur between the oxygen atoms in the hydroxyl groups of cellulose molecules and the hydrogen atoms in the seaweed polysaccharides, creating a stable intermolecular interaction [60]. Additionally, van der Waals forces, which are weak attractive forces between molecules, also contribute to the interaction between CNF and seaweed components. When nanocellulose is mixed with seaweed, it surrounds the seaweed structure and agglomerates to produce larger sizes. Better mechanical and thermal stability are found in aerogel with the inclusion of greater seaweed and CNF concentrations at high composition. Upon conducting meticulous 3D analysis, the opposite was observed. The skeletal structure was predominantly composed of seaweed biopolymer, while CNF played the role of encasing and reinforcing this structure, enhancing its mechanical properties and stability.

4. Conclusions

This study demonstrated that the incorporation of cellulose nanofibers (CNF) significantly reinforces the structural integrity of seaweed-based aerogels, reducing shrinkage and enhancing mechanical properties. Both biopolymers form aerogels differently: CNF aerogels create a thin network structure resembling an interconnected lattice of fibers. In contrast, aerogels from seaweed biopolymers take on a distinct form, comprising delicate thin sheets that mimic cellular structures or clusters, contributing to a unique and intricate architecture. Blending both

biopolymers resulted in a blended structure composed of thin network fibrils and thin sheets. Physical analysis revealed that CNF contributes to a denser network structure, which supports the aerogel

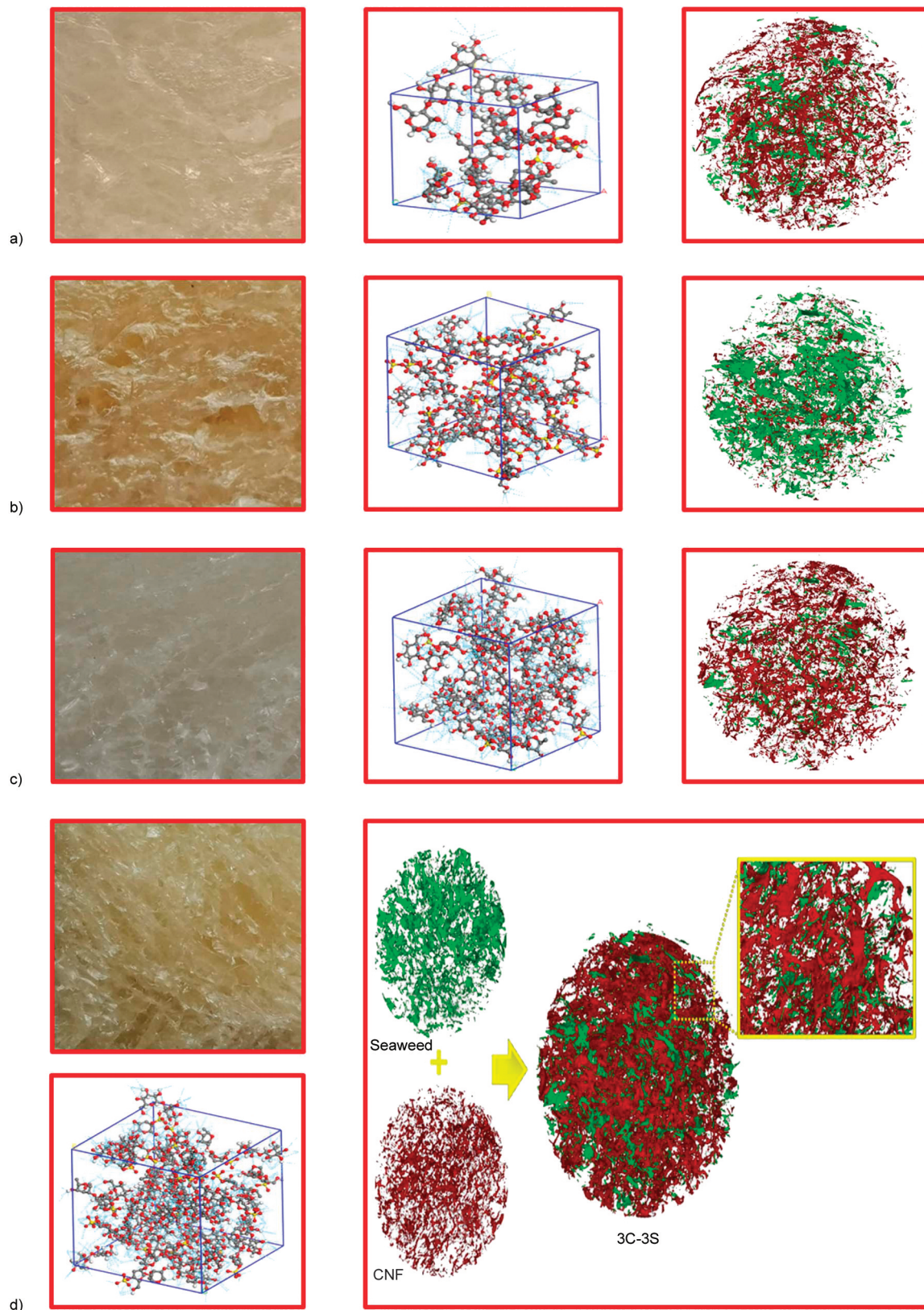


Figure 7. The real surface morphology, 3D interaction models, and 3D X-ray images of different composite aerogels: a) 1C-1S; b) 1C-3S; c) 3C-1S; and d) 3C-3S.

framework, leading to increased porosity and mechanical strength. In addition, CNF significantly contributes to the thermal stability of the composite aerogel. The interaction between the biopolymer used plays an important role in affecting the structure formation and aerogel mechanical properties. Computational molecular modeling and 3D X-ray imaging unveiled the interaction mechanisms between seaweed and CNF. Advanced 3D X-ray imaging revealed that the interaction between CNF and seaweed polysaccharides crucially involves the seaweed biopolymer forming the primary skeletal structure, with CNF serving as a reinforcing element. These findings enhance our understanding of the formation and biopolymer distribution within CNF-seaweed composite aerogels, offering valuable guidance for developing other composite aerogels tailored to specific applications.

Acknowledgements

The Deanship of Scientific Research (DSR) at King Abdulaziz University (KAU), Jeddah, Saudi Arabia has funded this project under grant no. (RG-18-166-43). The authors also extend their gratitude to those involved in the collaboration between Imam Abdulrahman Bin Faisal University and King Abdulaziz University in Saudi Arabia, the sabbatical program at Nasdeem Ventures Sdn. Bhd., as well as Universiti Sains Malaysia in Malaysia.

References

- [1] Abdul Khalil H. P. S., Yahya E. B., Jummaat F., Adnan A. S. S., Olaiya N. G., Rizal S., Abdullah C. K., Pasquini D., Thomas S.: Biopolymers based aerogels: A review on revolutionary solutions for smart therapeutics delivery. *Progress in Materials Science*, **131**, 101014 (2023). <https://doi.org/10.1016/j.pmatsci.2022.101014>
- [2] Ahmad A., Kamaruddin M. A., Abdul Khalil H. P. S., Yahya E. B., Muhammad S., Rizal S., Ahmad M. I., Surya I., Abdullah C. K.: Recent advances in nanocellulose aerogels for efficient heavy metal and dye removal. *Gels*, **9**, 416 (2023). <https://doi.org/10.3390/gels9050416>
- [3] Abdelmonem A. M., Zámbo D., Rusch P., Schlosser A., Klepzig L. F., Bigall N. C.: Versatile route for multifunctional aerogels including flaxseed mucilage and nanocrystals. *Macromolecular Rapid Communications*, **43**, 2100794 (2022). <https://doi.org/10.1002/marc.202100794>
- [4] Azimi B., Sepahvand S., Ismaeilimoghadam S., Kargarzadeh H., Ashori A., Jonoobi M., Danti S.: Application of cellulose-based materials as water purification filters; A state-of-the-art review. *Journal of Polymers and the Environment*, **32**, 345–366 (2024). <https://doi.org/10.1007/s10924-023-02989-6>
- [5] Basti A. T. K., Jonoobi M., Sepahvand S., Ashori A., Siracusa V., Rabie D., Mekonnen T. H., Naeijian F.: Employing cellulose nanofiber-based hydrogels for burn dressing. *Polymers*, **14**, 1207 (2022). <https://doi.org/10.3390/polym14061207>
- [6] Sepahvand S., Kargarzadeh H., Jonoobi M., Ashori A., Ismaeilimoghadam S., Varghese R. T., Chirayl C. J., Azimi B., Danti S.: Recent developments in nanocellulose-based aerogels as air filters: A review. *International Journal of Biological Macromolecules*, **246**, 125721 (2023). <https://doi.org/10.1016/j.ijbiomac.2023.125721>
- [7] Shao W., Han R., Niu J., Wang K., Liu S., Sun N., Li X., Han P., Cao Y., Wang Y., Zhang H., He J., Yu H., Liu F.: Electrospun-SiO₂-nanofiber-reinforced cellulose aerogel loaded with ZIF-67 for air filtration and formaldehyde adsorption. *Advanced Materials Technologies*, **9**, 2301395 (2024). <https://doi.org/10.1002/admt.202301395>
- [8] Oikonomou V. K., Dreier T., Sandéhn A., Mohammadi M., Christensen J. L., Tybrandt K., Dahl A. B., Dahl V. A., Bech M., Stavrinidou E.: Elucidating the bulk morphology of cellulose-based conducting aerogels with X-ray microtomography. *Advanced Materials Technologies*, **8**, 202300550 (2023). <https://doi.org/10.1002/admt.202300550>
- [9] Khalid M. Y., Al Rashid A., Arif Z. U., Ahmed W., Arshad H.: Recent advances in nanocellulose-based different biomaterials: Types, properties, and emerging applications. *Journal of Materials Research and Technology*, **14**, 2601–2623 (2021). <https://doi.org/10.1016/j.jmrt.2021.07.128>
- [10] Gupta P., Sathwane M., Chhajer M., Verma C., Grohens Y., Seantier B., Agrawal A. K., Maji P. K.: Surfactant assisted *in situ* synthesis of nanofibrillated cellulose/polymethylsilsesquioxane aerogel for tuning its thermal performance. *Macromolecular Rapid Communications*, **44**, 2200628 (2023). <https://doi.org/10.1002/marc.202200628>
- [11] Abdul Khalil H. P. S., Adnan A. S., Yahya E. B., Olaiya N. G., Safrida S., Hossain M. S., Balakrishnan V., Gopakumar D. A., Abdullah C. K., Oyekanmi A. A., Pasquini D.: A review on plant cellulose nanofiber-based aerogels for biomedical applications. *Polymers*, **12**, 1759 (2020). <https://doi.org/10.3390/polym12081759>

- [12] Noremylia M. B., Hassan M. Z., Ismail Z.: Recent advancement in isolation, processing, characterization and applications of emerging nanocellulose: A review. *International Journal of Biological Macromolecules*, **206**, 954–976 (2022).
<https://doi.org/10.1016/j.ijbiomac.2022.03.064>
- [13] Chamanehpour E., Thouti S., Rubahn H-G., Dolatshahi-Pirouz A., Mishra Y. K.: Smart nanofibers: Synthesis, properties, and scopes in future advanced technologies. *Advanced Materials Technologies*, **9**, 2301392 (2024).
<https://doi.org/10.1002/admt.202301392>
- [14] Ghalehno M. D., Yousefi H.: Green nanocomposite made from carboxymethyl cellulose reinforced with four types of cellulose nanomaterials of wheat straw. *Journal of Applied Polymer Science*, **139**, e52802 (2022).
<https://doi.org/10.1002/app.52802>
- [15] Chudasama N. A., Sequeira R. A., Moradiya K., Prasad K.: Seaweed polysaccharide based products and materials: An assessment on their production from a sustainability point of view. *Molecules*, **26**, 2608 (2021).
<https://doi.org/10.3390/molecules26092608>
- [16] Otero P., Carpena M., Garcia-Oliveira P., Echave J., Soria-Lopez A., Garcia-Pérez P., Fraga-Corral M., Cao H., Nie S., Xiao J., Simal-Gandara J., Prieto M. A.: Seaweed polysaccharides: Emerging extraction technologies, chemical modifications and bioactive properties. *Critical Reviews in Food Science and Nutrition*, **63**, 1901–1929 (2023).
<https://doi.org/10.1080/10408398.2021.1969534>
- [17] Abdul Khalil H. P. S., Lai T. K., Tye Y. Y., Rizal S., Chong E. W. N., Yap S. W., Hamzah A. A., Nurul Fazita M. R., Paridah M. T.: A review of extractions of seaweed hydrocolloids: Properties and applications. *Express Polymer Letters*, **12**, 296–317 (2018).
<https://doi.org/10.3144/expresspolymlett.2018.27>
- [18] Abdul Khalil H. P. S., Saurabh C. K., Tye Y. Y., Lai T. K., Easa A. M., Rosamah E., Fazita M. R. N., Syakir M. I., Adnan A. S., Fizree H. M., Aprilia N. A. S., Banerjee A.: Seaweed based sustainable films and composites for food and pharmaceutical applications: A review. *Renewable and Sustainable Energy Reviews*, **77**, 353–362 (2017).
<https://doi.org/10.1016/j.rser.2017.04.025>
- [19] Abdul Khalil H. P. S., Tye Y. Y., Saurabh C. K., Leh C. P., Lai T. K., Chong E. W. N., Nurul Fazita M. R., Mohd Hafiidz J., Banerjee A., Syakir M. I.: Biodegradable polymer films from seaweed polysaccharides: A review on cellulose as a reinforcement material. *Express Polymer Letters*, **11**, 244–265 (2017).
<https://doi.org/10.3144/expresspolymlett.2017.26>
- [20] Ramadas B. K., Rhim J-W., Roy S.: Recent progress of carrageenan-based composite films in active and intelligent food packaging applications. *Polymers*, **16**, 1001 (2024).
<https://doi.org/10.3390/polym16071001>
- [21] Autem Y., Bourgougnon N., Guihéneuf S., Perrot A.: Comparative study of effects of various seaweed parietal polysaccharides on rheological, mechanical and water-durability properties of earth-based materials. *Materials and Structures*, **56**, 108 (2023).
<https://doi.org/10.1617/s11527-023-02195-9>
- [22] Hermawan D., Lai T. K., Jafarzadeh S., Gopakumar D. A., Hasan M., Owolabi F. A. T., Sri Aprilia N. A., Rizal S., Abdul Khalil H. P. S.: Development of seaweed-based bamboo microcrystalline cellulose films intended for sustainable food packaging applications. *BioResources*, **14**, 3389–3410 (2019).
<https://doi.org/10.15376/biores.14.2.3389-3410>
- [23] Yahya E. B., Abdul Khalil H. P. S., Ahmad M. I., Rizal S., Muhammad S.: Cleaner approach of preparing antibacterial bioaerogel scaffolds using oil palm waste nanocellulose. *Industrial Crops and Products*, **191**, 115897 (2023).
<https://doi.org/10.1016/j.indcrop.2022.115897>
- [24] Li J., Wang Y., Zhang L., Xu Z., Dai H., Wu W.: Nanocellulose/gelatin composite cryogels for controlled drug release. *ACS Sustainable Chemistry and Engineering*, **7**, 6381–6389 (2019).
<https://doi.org/10.1021/acssuschemeng.9b00161>
- [25] Wang S., Wang F., Lu C., Ma S., Gu Y., Wang L.: Citral-loaded nanocellulose/sodium alginate aerogel packaging liner for fresh pork preservation. *Food Control*, **155**, 110031 (2024).
<https://doi.org/10.1016/j.foodcont.2023.110031>
- [26] Nasution H., Yahya E. B., Abdul Khalil H. P. S., Shaah M. A., Suriani A. B., Mohamed A., Alfatah T., Abdullah C. K.: Extraction and isolation of cellulose nanofibers from carpet wastes using supercritical carbon dioxide approach. *Polymers*, **14**, 326 (2022).
<https://doi.org/10.3390/polym14020326>
- [27] Guan Q-F., Yang H-B., Han Z-M., Ling Z-C., Yang K-P., Yin C-H., Yu S-H.: Plant cellulose nanofiber-derived structural material with high-density reversible interaction networks for plastic substitute. *Nano Letters*, **21**, 8999–9004 (2021).
<https://doi.org/10.1021/acs.nanolett.1c02315>
- [28] Ferdiansyah R., Abdassah M., Zainuddin A., Rachmaniar R., Chaerunisaa A. Y.: Effects of alkaline solvent type and pH on solid physical properties of carrageenan from *Eucheuma cottonii*. *Gels*, **9**, 397 (2023).
<https://doi.org/10.3390/gels9050397>
- [29] Mawardi I., Saharudin N. I., Ahmad A., Abdul Khalil H. P. S., Abdullah C. K., Yahya E. B.: Eco-friendly production and performance evaluation of water-resistant cellulose nanofiber bioaerogels. *Polymer Engineering and Science*, **64**, 733–748 (2023).
<https://doi.org/10.1002/pen.26580>

- [30] Azfaralariff A., Farahfaiqah F., Shahid M., Sanusi S. A., Law D., Mohd Isa A. R., Muhamad M., Tsui T. T., Fazry S.: *Marantodes pumilum*: Systematic computational approach to identify their therapeutic potential and effectiveness. *Journal of Ethnopharmacology*, **283**, 114751 (2022).
<https://doi.org/10.1016/j.jep.2021.114751>
- [31] Radakisnin R., Majid M. S. A., Jamir M. R. M., Jawaid M., Sultan M. T. H., Tahir M. F. M.: Structural, morphological and thermal properties of cellulose nanofibers from Napier fiber (*Pennisetum purpureum*). *Materials*, **13**, 4125 (2020).
<https://doi.org/10.3390/ma13184125>
- [32] Masruchin N., Amanda P., Kusumaningrum W. B., Suryanegara L., Nuryawan A.: Particle size distribution and yield analysis of different charged cellulose nanofibrils obtained by TEMPO-mediated oxidation. *IOP Conference Series: Earth and Environmental Science*, **572**, 012045 (2020).
<https://doi.org/10.1088/1755-1315/572/1/012045>
- [33] Gupta P., Singh B., Agrawal A. K., Maji P. K.: Low density and high strength nanofibrillated cellulose aerogel for thermal insulation application. *Materials and Design*, **158**, 224–236 (2018).
<https://doi.org/10.1016/j.matdes.2018.08.031>
- [34] Zhao S., Malfait W. J., Guerrero-Alburquerque N., Koebel M. M., Nyström G.: Biopolymer aerogels and foams: Chemistry, properties, and applications. *Angewandte Chemie International Edition*, **57**, 7580–7608 (2018).
<https://doi.org/10.1002/anie.201709014>
- [35] Shi J., Xiao Y., Fu G., Feng C., Hu J., Haegeman W., Liu H.: Calcareous silt earthen construction using biopolymer reinforcement. *Journal of Building Engineering*, **72**, 106571 (2023).
<https://doi.org/10.1016/j.jobbe.2023.106571>
- [36] Ahmad A., Omar K. M., Alahmadi A. A., Rizg W. Y., Bairwan R. D., Abdul Khalil H. P. S.: Bioadsorbent nanocellulose aerogel efficiency impregnated with spent coffee grounds. *International Journal of Biological Macromolecules*, **258**, 128746 (2024).
<https://doi.org/10.1016/j.ijbiomac.2023.128746>
- [37] Zainul R., Albadn Y. M., Yahya E. B., Manoharadas S., Saharudin N. I., Abdul Khalil H. P. S., Khan M. R., Jaber M.: Eco-friendly approach for nanocellulose isolation from agricultural wastes and the fabrication of bioaerogel scaffolds. *Express Polymer Letters*, **18**, 359–370 (2024).
<https://doi.org/10.3144/expresspolymlett.2024.27>
- [38] Popescu M. C., Dogaru B. I., Sun D., Stoleru E., Simionescu B. C.: Structural and sorption properties of bio-nanocomposite films based on κ -carrageenan and cellulose nanocrystals. *International Journal of Biological Macromolecules*, **135**, 462–471 (2019).
<https://doi.org/10.1016/j.ijbiomac.2019.05.194>
- [39] Yang Z., Yang H., Yang H.: Effects of sucrose addition on the rheology and microstructure of κ -carrageenan gel. *Food Hydrocolloids*, **75**, 164–173 (2018).
<https://doi.org/10.1016/j.foodhyd.2017.08.032>
- [40] Budtova T.: Cellulose II aerogels: A review. Springer, Amsterdam, **26**, 81–121 (2019).
<https://doi.org/10.1007/s10570-018-2189-1>
- [41] Lu Y., Gao R-N., Xiao S., Yin Y., Liu Q., Li J.: Cellulose based aerogels: Processing and morphology. in ‘Bio-based aerogels: Polysaccharide and protein-based materials’ (eds.: Thomas S., Pothan L. A., Mavelil-Sam R.) Royal Society of Chemistry, Cambridge, 25–41 (2018)
<https://doi.org/10.1039/9781782629979-00025>
- [42] Nishinari K., Kohyama K., Kumagai H., Funami T., Bourne M. C.: Parameters of texture profile analysis. *Food Science and Technology Research*, **19**, 519–521 (2013).
<https://doi.org/10.3136/fstr.19.519>
- [43] Chen J., Li H., Ma L., Jiang G., Li D., Wu Y., Shi X., Li D., Wang X., Deng H.: Chitosan-based recyclable composite aerogels for the photocatalytic degradation of rhodamine B. *Carbohydrate Polymers*, **273**, 118559 (2021).
<https://doi.org/10.1016/j.carbpol.2021.118559>
- [44] Savadekar N. R., Karande V. S., Vigneshwaran N., Bharimalla A. K., Mhaske S. T.: Preparation of nano cellulose fibers and its application in kappa-carrageenan based film. *International Journal of Biological Macromolecules*, **51**, 1008–1013 (2012).
<https://doi.org/10.1016/j.ijbiomac.2012.08.014>
- [45] Agostinho D. A. S., Paninho A. I., Cordeiro T., Nunes A. V. M., Fonseca I. M., Pereira C., Matias A., Ventura M. G.: Properties of κ -carrageenan aerogels prepared by using different dissolution media and its application as drug delivery systems. *Materials Chemistry and Physics*, **253**, 123290 (2020).
<https://doi.org/10.1016/j.matchemphys.2020.123290>
- [46] Thommes M., Blaschek W., Kleinebudde P.: Effect of drying on extruded pellets based on κ -carrageenan. *European Journal of Pharmaceutical Sciences*, **31**, 112–118 (2007).
<https://doi.org/10.1016/j.ejps.2007.02.010>
- [47] Kubovský I., Kačíková D., Kačík F.: Structural changes of oak wood main components caused by thermal modification. *Polymers*, **12**, 485 (2020).
<https://doi.org/10.3390/polym12020485>
- [48] Li J., Zhu Y., Wang C., Wei W., Liu Z., Tian Y., Zong P., Qiao Y., Qin S.: Golden seaweed tides from beach inundations as a valuable sustainable fuel resource: Fast pyrolysis characteristics, product distribution and pathway study on *Sargassum horneri* based on model compounds. *Algal Research*, **48**, 101888 (2020).
<https://doi.org/10.1016/j.algal.2020.101888>

- [49] Ma S., Chen L., Liu X., Li D., Ye N., Wang L.: Thermal behavior of carrageenan: Kinetic and characteristic studies. *International Journal of Green Energy*, **9**, 13–21 (2012).
<https://doi.org/10.1080/15435075.2011.617018>
- [50] Janković B., Manić N., Stojiljković D.: The gaseous products characterization of the pyrolysis process of various agricultural residues using TGA–DSC–MS techniques. *Journal of Thermal Analysis and Calorimetry*, **139**, 3091–3106 (2019).
<https://doi.org/10.1007/s10973-019-08733-4>
- [51] Surya I., Hazwan C. M., Abdul Khalil H. P. S., Yahya E. B., Suriani A. B., Danish M., Mohamed A.: Hydrophobicity and biodegradability of silane-treated nanocellulose in biopolymer for high-grade packaging applications. *Polymers*, **14**, 4147 (2022).
<https://doi.org/10.3390/polym14194147>
- [52] Kassab Z., Aziz F., Hannache H., Ben Youcef H., El Achaby M.: Improved mechanical properties of κ -carrageenan-based nanocomposite films reinforced with cellulose nanocrystals. *International Journal of Biological Macromolecules*, **123**, 1248–1256 (2019).
<https://doi.org/10.1016/j.ijbiomac.2018.12.030>
- [53] Hamdan M. A., Ramli N. A., Othman N. A., Mohd Amin K. N., Adam F.: Characterization and property investigation of microcrystalline cellulose (MCC) and carboxymethyl cellulose (CMC) filler on the carrageenan-based biocomposite film. *Materials Today: Proceedings*, **42**, 56–62 (2021).
<https://doi.org/10.1016/j.matpr.2020.09.304>
- [54] Nair S. S., Zhu J., Deng Y., Ragauskas A. J.: High performance green barriers based on nanocellulose. *Sustainable Chemical Processes*, **2**, 23 (2014).
<https://doi.org/10.1186/s40508-014-0023-0>
- [55] Li W., Sun B., Wu P.: Study on hydrogen bonds of carboxymethyl cellulose sodium film with two-dimensional correlation infrared spectroscopy. *Carbohydrate Polymers*, **78**, 454–461 (2009).
<https://doi.org/10.1016/j.carbpol.2009.05.002>
- [56] Pandey S. K., Manogaran D., Manogaran S., Schaefer H. F.: Quantification of hydrogen bond strength based on interaction coordinates: A new approach. *Journal of Physical Chemistry A*, **121**, 6090–6103 (2017).
<https://doi.org/10.1021/acs.jpca.7b04752>
- [57] Ahmed I., Jhung S. H.: Applications of metal-organic frameworks in adsorption/separation processes *via* hydrogen bonding interactions. *Chemical Engineering Journal*, **310**, 197–215 (2017).
<https://doi.org/10.1016/j.cej.2016.10.115>
- [58] Adam F., Othman N. A., Yasin N. H. M., Cheng C. K., Azman N. A. M.: Evaluation of reinforced and green bioplastic from carrageenan seaweed with nanocellulose. *Fibers and Polymers*, **23**, 2885–2896 (2022).
<https://doi.org/10.1007/s12221-022-4006-6>
- [59] Liu X., Liu Q., Wang S., Liu Z., Yang G., Wang H., Xiong W., Li P., Xu F., Xi Y., Kong F.: Effect of functional group and structure on hydrophobic properties of environment-friendly lignin-based composite coatings. *International Journal of Biological Macromolecules*, **215**, 132–140 (2022).
<https://doi.org/10.1016/j.ijbiomac.2022.06.055>
- [60] Yahaya W. A. W., Azman N. A. M., Adam F., Subramaniam S. D., Abd Hamid K. H., Almajano M. P.: Exploring the potential of seaweed derivatives for the development of biodegradable plastics: A comparative study. *Polymers*, **15**, 2884 (2023).
<https://doi.org/10.3390/polym15132884>